JOURNAL OF VIROLOGY, June 2011, p. 5606–5617 Vol. 85, No. 11
0022-538X/11/$12.00 doi:10.1128/JVI.01502-10

Adaptation of an ICAM-1-Tropic Enterovirus to the Mouse Respiratory Tract▽

Eric S. Wang,† Elena Dobrikova, Christian Goetz, Andrew T. Dufresne, and Matthias Gromeier*

Division of Neurosurgery, Department of Surgery, Duke University Medical Center, Durham, North Carolina 27710

Received 19 July 2010/Accepted 17 March 2011

Respiratory tract (RT) infections by members of the enterovirus (EV) genus of the *Picornaviridae* family are the most frequent cause for the common cold and a major factor in the exacerbation of chronic pulmonary diseases. The lack of a practical small-animal model for these infections has obstructed insight into pathogenic mechanisms of the common cold and their role in chronic RT illness and has hampered preclinical evaluation of antiviral strategies. Despite significant efforts, it has been difficult to devise rodent models that exhibit viral replication in the RT. This is due mainly to well-known intracellular host restrictions of EVs with RT tropism in rodent cells. We report the evolution of variants of the common-cold-causing coxsackievirus A21, an EV with tropism for the human intercellular adhesion molecule 1 (hICAM-1), through serial passage in the lungs of mice transgenic for the *hICAM-1* gene. This process was accompanied by multiple changes in the viral genome, suggesting exquisite adaptation of hICAM-1-tropic enteroviruses to the specific growth conditions within the RT. *In vivo* mouse RT-adapted, variant coxsackievirus A21 exhibited replication competence in the lungs of *hICAM-1* transgenic mice, providing a basis for unraveling EV-host interactions in the mouse RT.

The common cold (acute nasopharyngitis) is a frequent ailment, primarily of viral etiology, recognized since antiquity. The incidence in adults and children ranges from 2 to 4 and 6 to 8 cases, respectively, per person per year. The economic impact of viral, noninfluenza respiratory tract (RT) infections has been estimated at ~$40 billion/year in the United States alone (16). A majority of viral infections are due to members of the enterovirus (EV) genus of the *Picornaviridae* family recognizing hICAM-1 as a receptor (20, 39, 40). These comprise 88 major-group human rhinoviruses (HRVs) and coxsackievirus A (CAV) serotypes 1, 11, 13, 15, and 17 to 24. EV RT infections cause transient, benign symptoms, such as rhinorrhea, sneezing, and sore throat, but they are major factors in the exacerbation of asthma (28, 35) and chronic obstructive pulmonary disease (COPD) (37, 38). Curiously, viral replication is modest and host cell destruction in the RT is absent (21, 44), indicating a role of host inflammatory reactions rather than overt tissue damage in pathogenesis (33, 34). The significant public health impact of EV RT infections inspired many efforts to develop animal models. Since natural susceptibility is restricted to higher primates (12), these approaches were based on adapting EVs to rodents. HRVs that use the low-density lipoprotein receptor (LDL-R) for host cell entry spontaneously infect mouse L fibroblasts (47) and exhibit very modest replication in wild-type (wt) BALB/c mice (46). This suggests that these viruses either use the murine LDL-R or another murine cell surface molecule for host cell attachment and entry. More targeted, recent efforts focused on supplying authentic human receptors, e.g., with mice transgenic for the *hICAM-1* gene (*hICAM-1* tg mice) (1).

However, despite circumventing host-range determinants for attachment and entry, producing a viable murine model for EV RT infection has met substantial obstacles. The reason for this is inherently deficient replication in the murine RT. All HRVs, independent of receptor choice, exhibit poor growth in mouse cells. Growth of HRV2 improved upon genetic adaptations after serial passage in mouse L fibroblasts (47), which were shown to map to the nonstructural proteins 2B/2C (32). Similarly, poor replication of HRVs 16 and 39 in mouse L fibroblasts expressing hICAM-1 significantly improved upon acquisition of adaptation mutations in viral nonstructural proteins 2B, 2C, or 3A (23, 24).

We report here the generation of an hICAM-1-tropic EV strain with replication competence in the murine RT. Our efforts focused on the laboratory strain CAV21(Kuykendall), referred to as CAV21 here. A number of basic observations support the use of CAV21 over HRVs in mouse models for RT replication. The natural histories of CAV21 and HRV respiratory infection are similar (3, 27), and their aerosols produce identical illnesses in human subjects (4, 10). While most HRVs exhibit a marked preference for growth at 33.5°C with significant replication deficits at 37.0°C (the prevailing temperature in mouse lung is even higher) (8), CAV21 grows equally well at either temperature. Lastly, CAV21 readily replicates in mixed primary explant cultures from *hICAM-1* tg mouse embryos, modestly grows in the central nervous system (CNS), and causes histopathological lesions in adult *hICAM-1* tg mice (14). Yet, our studies revealed that wt CAV21, which is replication competent in mouse L fibroblasts, shares the severe growth deficits of HRVs 16 and 39 in mouse primary RT epithelial cells expressing hICAM-1.

We devised a serial *in vivo* adaptation strategy to select for CAV21 variants with replication competency in the lungs of *hICAM-1* tg mice. This produced an adaptation genotype me-

* Corresponding author. Mailing address: Department of Surgery, Duke University Medical Center, Box 3020, Sands 201, Durham, NC 27710, Phone: (919) 668-6205. Fax: (919) 681-4991. E-mail: grome001@mc.duke.edu.

† Present address: Biomedical Sciences Graduate Program, Department of Pathology, University of California, San Francisco, 513 Parnassus Ave, Box 0452, Rm HSE-1285, San Francisco, CA 94143.

▽ Published ahead of print on 30 March 2011.

TABLE 1. Primers used in this study

No.	Name	5′→3′ sequence	Position in wt CAV21 genome[a]
1	5′ T7	TGGCGGCCGCGGAAATCCG	NA
2	3′ EcoRI	AAGGAATTCGGGAAGGGATAC	88–106
3	5′ EcoRI	CCCGAATTCCTTTAGAAGCTTATC	97–120
4	5′ hICAM-1	GGAAGCTTCGCTATGGCTCCCAGC	NA
5	3′ hICAM-1	CGTCTAGAGATAGGTTCAGGGAGG	NA
6	5′ 7	CAGCTCTGGGGTTGTTCC	7–24
7	5′ B07	CCTGTTTTGTATCCCTTCCC	80–99
8	5′ 441	GAGTCCTCCGGCCCCTGAATGC	439–460
9	5′ 721	GGGAGCTCAAGTTTCAACGC	716–735
10	3′ 721	TTGAGCTCCCATTTGCACTG	706–725
11	5′ 779	GGCAGCCAATGGATCCACCATT	767–788
12	3′ 779	GGTGGATCCATTGGCTGCCACG	764–785
13	3′ 1045	GAATCATTTATGTAAGTGGG	1035–1054
14	5′ 1169	CCAGATTGTTTGAAGGACATGGG	1167–1189
15	3′ 1691	CCCATTGAACTCTGTACACATGG	1684–1706
16	5′ 1697	GTTCAATGGGTTGAGAAACATC	1697–1718
17	5′ 2121	GGTAAACTGCTCCTCAGC	2115–2132
18	3′ 2206	CCCTAGGTCCCAGATGATGTG	2190–2210
19	5′ 2685	GTCATTCTTTGGGAGAGCTGC	2675–2695
20	3′ 2770	GTAATATTCCATATGTTGAAATGC	2750–2773
21	3′ 3004	GGAGGTGCATTTCCATACATG	2996–3016
22	5′ 3160	GCAGTTAGAGCAGTAAACCGC	3162–3182
23	3′ 3490	GGCGATGGTATCAGTTCCCTG	3489–3509
24	5′ 3609	CGACTACTATCCAGCAAGATACC	3608–3630
25	3′ 3683	CCTCAGTATCCCACCGCAGTC	3672–3692
26	5′ 3994	CGATCCTTGCAACACTAGC	3985–4003
27	5′ 4332	GGTTAGCAGTCCAGTCCC	4333–4350
28	3′ 4380	CCACAGCGTATAATGGTGC	4359–4377
29	5′ 4950	GGAAAGGCCTTGCAATTAATGG	4947–4968
30	3′ 5060	GGCTTCCATGCAATTGCCGATATTGG	5041–5066
31	3′ 5215	CCTTTCTAGTTGAATCTGGC	5218–5237
32	5′ 5550	GATGGGAAAGAAGTAGAGATCC	5550–5571
33	3′ 5604	GGTGATCTCAAGATTGGTTCCC	5600–5621
34	5′ 5988	GTGGGGTACCCCATTATAAATGC	5985–6007
35	3′ 6570	GCTGATCCTGTCACCACACCTGG	6555–6577
36	5′ 6641	CGCTTTTGACTACACAGGG	6641–6659
37	3′ 6771	CTGAGTGAGGCATCATACCC	6657–6676
38	5′ 7305	CTCTACATTGTACCGCCGATGGCTCG	7301–7326
39	3′ 3-UTR	CCCCTACAACAGTATAACCC	7364–7383

[a] NA, not applicable.

diating distinct viral replication dynamics in susceptible cell lines *in vitro* and active replication and viral translation in RT epithelium of *hICAM-1* tg mice. Similar to mouse-adapted HRVs, genetic alterations acquired upon CAV21 adaptation to growth in the murine RT affected nonstructural proteins encoded in the P2 region of the viral genome. In addition, adaptation involved changes of capsid proteins that may alter virus–hICAM-1 interactions and hICAM-1 signaling upon virus binding.

MATERIALS AND METHODS

Viruses, animals, immunohistochemistry, and histopathology. An infectious CAV21(Kuykendall) clone, kindly provided by E. Wimmer (Stony Brook University, NY), was rederived, propagated, and purified as described previously (14). To facilitate the derivation of CAV21 recombinants, an EcoRI endonuclease restriction site was engineered in the viral 5′ untranslated region (UTR) by PCR of the CAV21 cDNA template with primer pairs 1/2 and 3/12 (Table 1). The resulting fragments were digested with NotI and BamHI and inserted into the corresponding sites of the CAV21 cDNA. *hICAM-1* tg mice, founder line 4, have been characterized in detail (14). All procedures involving vertebrate animals were reviewed and approved by the Institutional Animal Care and Use Committee. For intranasal (i.n.) inoculations, mice were anesthetized with isoflurane in a Matrix3000 gas anesthesia apparatus and suspended from their front incisors, and 2 or 5 droplets each of 10 μl were applied to both nares for a total delivery of 20 μl or 50 μl, respectively. The animals were left suspended for ~1 min and returned to their cages. For intratracheal (i.t.) inoculations, after deep sedation with intraperitoneal ketamine-xylazine, an ~8-mm incision was applied to expose the thyroid gland and to prepare the underlying trachea for injection with a 28G1/2′ insuject syringe (Becton Dickinson). Virus suspension (30 μl) was slowly instilled into the trachea. Aspiration of the inoculum was carefully inspected to ensure proper delivery. Following the inoculation procedure, the incision was stapled and animals were returned to their cages. At the time of euthanasia, animals were given an intraperitoneal injection of 250 mg pentobarbital/kg body weight. The carcasses were perfused with cold, sterile phosphate-buffered saline (PBS), and the lungs were removed for further analysis. Immunohistochemical analysis of hICAM-1 expression in the RT was performed as described previously (14). For histopathology, the lungs were instilled with 4% paraformaldehyde (in PBS). The perfused and fixed lungs were removed and processed for paraffin sectioning as described before (14).

Tissue processing, virus quantification, and serial *in vivo* passage. For homogenization and virus reisolation, dissected lungs were freeze-thawed and weighed, Dulbecco's modified Eagle's medium (DMEM; Invitrogen) containing 500 IU/ml penicillin, 500 μg/ml streptomycin, and 5 μg/ml amphotericin B (all

Invitrogen) was added at 5:1 (volume:weight), and the material was thoroughly homogenized at 4°C in an automated homogenizer (PRO Scientific). The lung homogenate was freeze-thawed and briefly centrifuged to collect large debris, and the supernatant was tested by standard plaque assay as described previously (14). Tests of virus recovery from the pelleted debris in the lungs of 10 *hICAM-1* tg or non-tg mice each revealed that, consistently, >95% of total recovered virus was present in the supernatant. Therefore, the indicated virus titers represent infectious material recovered from the homogenate supernatant. For serial passage of CAV21 in *hICAM-1* tg lungs, 500 μl of the homogenate supernatant was used to infect HeLa H1 cells grown to 70% confluence in 60-mm dishes (Greiner). The cells were incubated at 37°C until all cells exhibited signs of cytopathic effects. After being freeze-thawed twice, the cell lysates were collected and centrifuged at 12,000 rpm for 30 min to remove cellular debris. The resulting homogenate was analyzed by plaque assay to quantify virus in preparation for subsequent i.t. instillation into *hICAM-1* tg mice.

ICAM-1 antibody assays. ICAM-1 *in vitro* blockade in HeLa H1 cell monolayers and *in vivo* blockade with i.t. infection of *hICAM-1* tg mice were carried out as follows. HeLa H1 cell monolayers grown in 24-well plates (Greiner) were pretreated for 1 h at 37°C with 40 or 4 nM anti-ICAM-1 antibody (clone RR1/1; Invitrogen), 40 nM isotype-controlled nonspecific mouse IgG1, or medium alone. Thereafter, the media were aspirated and replaced with 200 μl of suspension containing virus at a multiplicity of infection (MOI) of 0.5. The plate was gently rocked at room temperature for 30 min, and the wells were rinsed twice to remove unbound virus and overlaid with DMEM before incubation at 37°C. Cultures were frozen immediately after rinsing to measure virus bound to cells at 0 h postinfection (p.i.) and after 8 h p.i. at 37°C. The cultures were freeze-thawed twice, and cell lysates were subjected to plaque assay to determine viral progeny titers as previously described (14). For animal experiments, virus suspensions were prepared that contained 2×10^5 PFU of CAV21 or CAV-RTA (respiratory tract adapted) and either 40 nM RR1/1 antibody or 40 nM nonspecific IgG1.

hICAM-1-expressing mouse cell lines, serial passage *in vitro*, one-step growth curves, and hICAM-1 signaling assays. Mouse L fibroblasts and La-4 respiratory epithelial cells (both obtained from ATCC) were grown as instructed by the provider and transfected with hICAM-1 expression plasmid cDNA using standard methods described elsewhere (13). The hICAM-1 expression plasmid was generated as follows. The hICAM-1 open reading frame (ORF) was amplified with reverse transcription-PCR (RT-PCR) from total HeLa H1 cell RNA isolated with Trizol reagent (Invitrogen) according to the manufacturer's instructions with primers 4 and 5 (Table 1). The resulting PCR fragment was digested with restriction endonucleases XbaI and HinDIII and inserted into pcDNA3.1 (Invitrogen) previously digested with the same enzymes. Stable mouse L and La-4 cell lines were obtained by growing transfected cells in the presence of neomycin and clonal selection by following standard procedures. Expression of hICAM-1 was confirmed by FACS analysis (ICAM-L5 cells) (see Fig. 2A) or antigen capture/immunoblot (ICAM-La-4 cells) (see Fig. 2C). For *in vitro* passage, ICAM-La-4 cells were grown to ~70% confluence in 60-mm culture dishes (Greiner) and infected with CAV21 at a multiplicity of infection of 10. Following 48 h of incubation at 37°C, the cells were freeze-thawed twice, and the resulting lysate was used to infect HeLa H1 cells to amplify the inoculum. Infected HeLa H1 cells were incubated at 37°C until full cytopathic effects were evident, and cells were freeze-thawed thereafter. One milliliter of infected HeLa H1 cell lysate was used to overlay ICAM-La-4 cells for a subsequent round of infection. The procedure was repeated 10 times with alternate ICAM-La-4/HeLa H1 passages and 5 times with serial ICAM-La-4 passages. Virus obtained after the final passage was used for plaque purification by standard methods. One-step growth curves were established as previously described (17). To analyze hICAM-1 signaling upon CAV21 binding, HeLa H1 cells were serum starved for 48 h and infected at an MOI of 10. At defined intervals, the cells were rinsed with PBS, lysed, and processed for immunoblots with antibodies against Erk1/2, phospho-Erk1/2, and phospho-Akt(Thr308) (all Cell Signaling) as described before (19).

FACS and immunoblots. Fluorescence-activated cell sorting (FACS) analysis of ICAM-L5 cells was conducted as follows. Stable, clonal selected ICAM-L5 cells were collected by scraping from culture flasks, washed, and pelleted by centrifugation. HeLa H1 cells, wt L cells, and ICAM-L5 cells (500,000 cells each) were FACS analyzed in the presence of fluorescein isothiocyanate (FITC)-labeled anti-ICAM-1 antibody (Calbiochem; catalog number 217607) (2) or isotype-matched, nonspecific mouse IgG1 control (BD Biosciences; catalog number 555748) following standard procedures. A solid-phase antigen-capture/immunoblot procedure to detect hICAM-1 expression in transduced cells has been described before (14). Immunoblots for translation factors and viral proteins were carried out as reported previously (13).

Sequencing of viral genomes and rederivation of cloned viruses. Sequencing of viral genomes followed earlier published procedures (17). Briefly, plaque purified virus or mixed virus populations recovered after serial *in vitro* passage in ICAM-La-4 cells or serial *in vivo* passage in the lungs of *hICAM-1* tg mice were propagated in HeLa H1 cells. Total RNA was purified from infected HeLa H1 cell lysates with Trizol reagent (Invitrogen). Staggered primers 15, 21, 30, and 39 (Table 1) were used for reverse transcription of discrete regions of the viral genome. Primer pairs 6/15, 8/21, 17/30, and 27/39 (Table 1) were used to generate overlapping PCR products covering >99% of the viral genome (we were unable to determine the sequence of the ~30 5′-most and 3′-most nucleotides of the viral RNA). A variable combination of primers 6 to 39 (Table 1) was used for sequencing of the RT-PCR products. All sequence alterations identified in Fig. 3 were evident when employing at least 2 distinct primers. ICAM-La-4-adapted CAV21, CAV-RTA, and CAV-RTB (respiratory tract adapted with wild-type CAV21 capsid) were cloned as follows. RT-PCR of total RNA isolated from HeLa H1 cells infected with the respective isolates was performed with primers 12, 18, and 30. Primer pairs 7/12, 11/18, and 22/30 were used to PCR amplify portions of the CAV21 genome from these RT-PCR reactions. For generating CAV-RTA, PCR fragments encompassing the 5′ UTR (nucleotides [nt] 80 to 785), parts of VP2/VP3 (nt 767 to 2210), and parts of VP1/2A/2C (nt 3162 to 5069) were digested with EcoRI/BamHI, BamHI/AvrII, or XhoI/StuI, respectively, and inserted into the wt CAV21 cDNA. To derive CAV-RTB, we digested CAV-RTA cDNA with BamHI (nt 777) and AvrII (nt 2204) and inserted the corresponding fragment from wt CAV21. ICAM-La-4-adapted virus was cloned with PCR fragments encompassing parts of VP2/VP3 (nt 767 to 2210) and VP1/2A/2C (nt 3162 to 5069) as described above. Mutant viruses were derived after transfection of HeLa H1 cells with infectious *in vitro* transcript RNA as described before (17).

Viral protein expression in mouse lungs. To assess expression of viral, nonstructural proteins in the lungs of *hICAM-1* tg mice or their non-tg peers, male 16- to 20-week-old mice were inoculated with 2×10^7 PFU of CAV21 or CAV-RTA (in 30 μl) by the i.t. route as described above. Mice were euthanized as described above, and their carcasses were perfused with 10 ml ice-cold PBS. The lungs were dissected and immediately thereafter snap-frozen on dry ice. The frozen tissues were thawed in 5 volumes (weight per volume) of lysis buffer (50 mM HEPES [pH 7.4], 150 mM NaCl, 0.5% NP-40, 10% glycerol, 1 mM EDTA, 5 mM EGTA, 2.5 mM dithiothreitol [DTT]) supplemented with Complete protease inhibitor cocktail (Roche) and Halt phosphatase inhibitor cocktail (Pierce). The lungs were then homogenized thoroughly in an automated homogenizer. The resulting lysate was incubated for 30 min at 4°C and frozen at −80°C thereafter. After thawing on wet ice, the homogenates were spun 10 min at $1{,}000 \times g$ to remove gross debris. The supernatants from the first spin were centrifuged at high speed ($20{,}000 \times g$) for 10 min. The resulting pellets containing membrane fractions were resuspended in 2 volumes of lysis buffer. The final supernatants and the resuspended pellet fractions were analyzed by immunoblotting as follows. For supernatant samples, 100 μg of total protein per lane (protein concentrations were determined by Bradford assay) was loaded for analysis by SDS-PAGE. For pellet samples, since Bradford assays cannot be used due to the nonhomogeneous state of the resuspended samples, 15 μl was loaded per lane. This amount yielded a level of characteristic background bands identical to that of lysate from supernatants, corresponding to 100 μg of total protein. Immunoblots were carried out with a rabbit polyclonal antibody against poliovirus 3D (a gift of E. Wimmer) according to procedures described before (13).

RESULTS

Intratracheal administration of CAV21 improves RT delivery. To test replication competence of CAV21 in the murine RT, we conducted experimental RT infections of *hICAM-1* tg mice or their non-tg littermates and quantified virus recovered from excised lung. We used *hICAM-1* tg strain 4 for our studies, which exhibits hICAM-1 organ type-specific expression similar to that of humans (14). Immunohistochemical analyses of the lungs of *hICAM-1* tg mice revealed an hICAM-1 expression pattern consistent with expression on the apical surface of RT epithelial cells (Fig. 1A).

Our approach is complicated by the fact that, due to virus administration to the RT, the original inoculum cannot be distinguished from viral progeny. Also, for anatomical reasons, it is difficult to assess viral presence in the upper RT (the primary site for replication in humans) in mice. Virus admin-

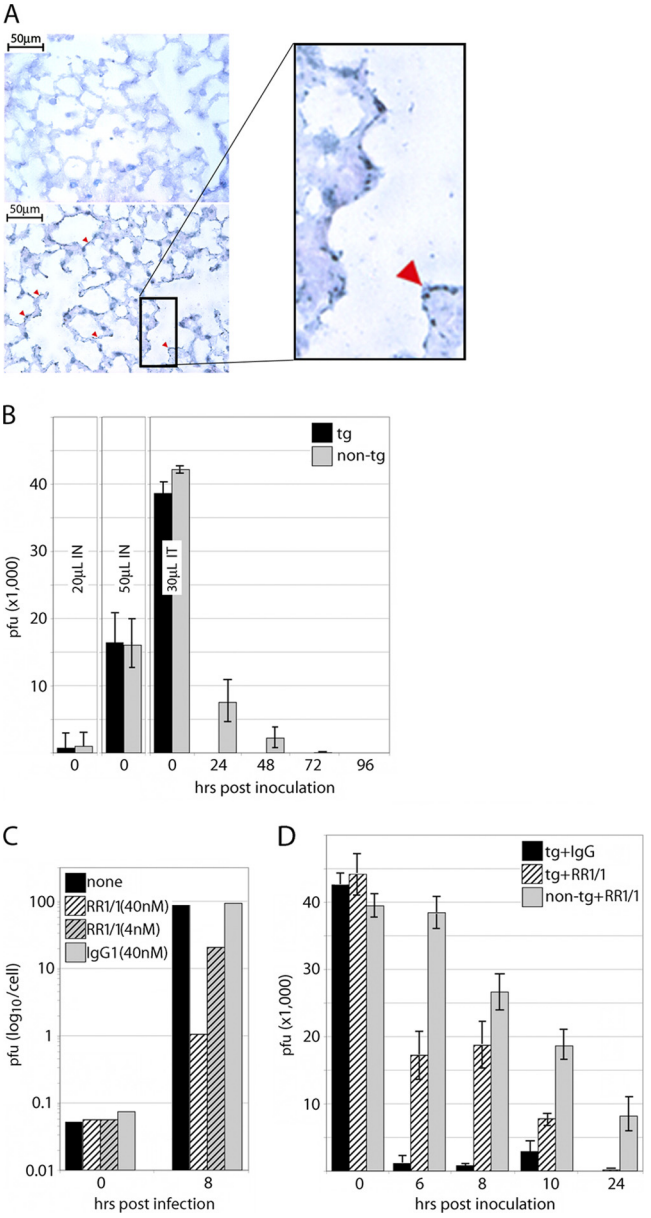

FIG. 1. CAV21 recovery from lungs after i.t. inoculation in *hICAM-1* tg mice. (A) Immunohistochemical detection of hICAM-1 expression in RT epithelium of *hICAM-1* tg mice (bottom) and non-tg littermates (top). Red arrowheads indicate the blue chromogenic substrate indicative of hICAM-1 expression in RT epithelium. (B) Virus recovered from lungs of groups of mice ($n = 4$ mice per group) inoculated with 2×10^5 PFU of CAV21. Groups of *hICAM-1* tg mice or non-tg littermates ($n = 4$ mice per group) were inoculated with CAV21 as described in Materials and Methods and tested for virus recovery from lungs at the intervals shown. IN, intranasal; IT, intratracheal. The values represent the average recovered amounts of virus from the animals in each group; bars indicate standard deviations. (C) CAV21 propagation in HeLa H1 cells pretreated with medium alone or medium containing the indicated antibodies. (D) Virus recovered from lungs of groups of male *hICAM-1* tg or non-tg mice ($n = 4$) inoculated i.t. with a suspension containing 2×10^5 PFU CAV21 and the indicated antibodies (40 nM).

istration techniques were optimized to cope with these limitations. First, because virus replication is tested in lungs but intranasal (i.n.) delivery of virus to the lung is inefficient (only ~0.5% or ~8% of the inoculum is recovered immediately after i.n. administration of 20 μl or 50 μl, respectively [Fig. 1B]), we performed intratracheal (i.t.) inoculations instead. This method permitted instant recovery of ~20% of the inoculum (Fig. 1B). Intratracheal delivery improved accuracy and produced remarkably even recovery across individual animals in experimental groups in all subsequent assays. Second, inoculation titers were limited to 2×10^5 PFU to minimize input virus; very low viral titers are sufficient to initiate RT infection in humans (9).

CAV21 is rapidly cleared from the RT of *hICAM-1* tg mice. For measurements of recovered virus, dissected mouse lungs were processed as described in Materials and Methods, and the resulting homogenate was tested by plaque assay. Total titers isolated from lungs per animal were averaged in groups of 4 animals. Virus recovery 5 min after i.t. inoculation was undistinguishable between tg mice and their non-tg littermates (Fig. 1B). In the latter, ~3.5% of the inoculum was isolated after 24 h, with diminishing returns until 72 h after injection (Fig. 1B). Intriguingly, a mere <0.0025% of the inoculum was recovered from tg mice at 24 h, and no virus was isolated thereafter (Fig. 1B). Accelerated clearance of CAV21 from the lungs of *hICAM-1* tg mice suggested a receptor-mediated event, e.g., uptake and eclipse in hICAM-1-expressing RT epithelial cells. To test this directly, we employed receptor blockage with anti-ICAM-1 antibody.

Specific inhibition of HRV attachment and replication with anti-ICAM-1 antibodies has been shown before *in vitro* (6) and in chimpanzees or human volunteers (7, 25). We recapitulated this effect with monoclonal anti-ICAM-1 antibody RR1/1, previously used to block HRV binding *in vitro* (5). Pretreatment of HeLa H1 cells with RR1/1 resulted in an ~80-fold or ~4-fold reduction of progeny at 8 h postinfection with 40 nM or 4 nM antibody, respectively (Fig. 1C). To evaluate the possibility of CAV21 binding to and eclipse in murine RT epithelial cells, we evaluated virus recovery in the presence of RR1/1 anti-ICAM-1 antibody in both *hICAM-1* tg and non-tg animals. For controls, *hICAM-1* tg mice were inoculated with CAV21 in the presence of isotype-matched nonspecific mouse IgG. Since receptor binding and eclipse of virus in *hICAM-1* tg mice are likely to occur prior to 24 h after inoculation (producing the diminished recovery at 24 h [Fig. 1B]), we tested intervals of 6, 8, 10, and 24 h after i.t. virus inoculation in groups of four animals each (Fig. 1D).

Clearance of CAV21 from the RT of *hICAM-1* tg mice was rapid. Six hours after virus inoculation, only ~0.5% of the recoverable inoculum was lost from non-tg animals, but ~95% of virus was cleared from tg mice (Fig. 1D, tg+IgG). The addition of 40 nM RR1/1 to the i.t. inoculum substantially elevated virus recovery from inoculated lungs in *hICAM-1* tg mice (Fig. 1D, tg+RR1/1). At 6 h postinoculation, virus recovery was increased ~10-fold compared to that in animals injected with virus in the presence of nonspecific IgG (Fig. 1D). The effect of the anti-ICAM-1 antibody waned with time. It was reduced to ~3.5-fold enhanced recovery by 10 h and was insignificant after 24 h (Fig. 1D). Similar recovery after 24 h with or without RR1/1 suggests that the anti-ICAM-1 antibod-

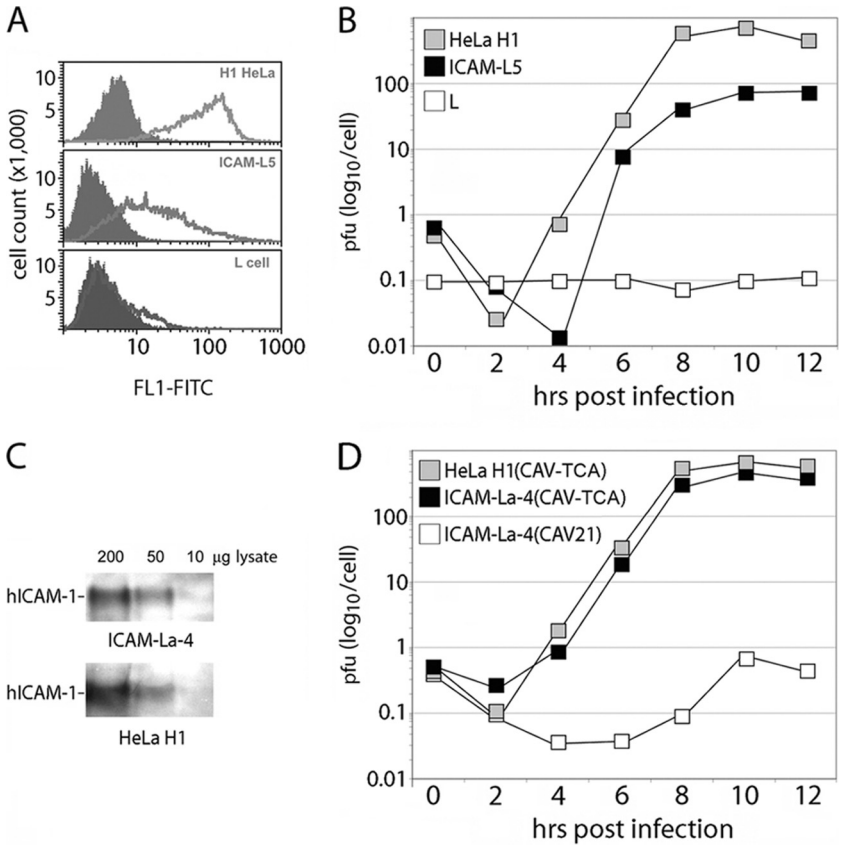

FIG. 2. *In vitro* adaptation of CAV21 to growth in ICAM-La-4 cells. (A) FACS analysis of HeLa H1 cells, mouse L fibroblast cells, or an L cell line expressing hICAM-1 (ICAM-L5). Filled graphs represent the FACS signal obtained with a control isotype-matched nonspecific mouse IgG1; line graphs show FACS signal with an FITC-labeled anti-ICAM-1 antibody. (B) One-step growth kinetics of CAV21 in the indicated cell lines. The data show one representative assay of two independent experiments. (C) Solid-phase antigen capture immunoblot of hICAM-1 in La-4 cells stably transduced with hICAM-1 (ICAM-La-4) and HeLa H1 cells. Decreasing amounts of cell lysate were analyzed. (D) One-step growth curves of wt CAV21 and a cloned 10-passage adapted variant (CAV-TCA) in the indicated cell lines. Representative data from one series of two independent experiments are shown.

ies had no influence on recovery of CAV21 from non-tg animals (Fig. 1D, non-tg+RR1/1). Also, the addition of control, isotype-matched mouse IgG did not alter virus recovery in *hICAM-1* tg mice, because titers obtained after 24 h were equally low in animals inoculated without antibody (Fig. 1B). Our data suggest that the rapid loss of CAV21 from i.t. injected *hICAM-1* tg mice is due to interactions with hICAM-1 in the RT. CAV21 may readily bind to hICAM-1 in the RT and undergo eclipse. While these events may indicate successful CAV21 entry into RT epithelial cells of *hICAM-1* tg mice, the lack of significant virus recovery beyond 10 h after i.t. inoculation suggested poor virus replication in such cells.

***In vitro* adaptation of CAV21 to mouse RT epithelial cells.** Since our data indicated that CAV21 enters *hICAM-1* tg mouse RT epithelial cells in an hICAM-1-mediated event, CAV21's obvious growth deficit in mouse lungs may be due to host/cell-type-specific restrictions of virus replication. Although, in contrast to hICAM-1-tropic HRVs (23, 24), CAV21 grows efficiently in mouse L fibroblasts expressing hICAM-1 (ICAM-L5) (Fig. 2A, B), these are nonrepresentative targets that may not accurately predict virus competency in RT epithelium. Therefore, we generated mouse RT epithelial cells (La-4) expressing hICAM-1 (ICAM-La-4 cells) (Fig. 2C). La-4 cells are of epithelial origin, derived from induced mouse pulmonary adenoma (41). La-4 cells retain characteristics of the RT epithelium, grow at lower rates than most transformed cells, do not form soft agar colonies, and are nontumorigenic in isogenic animals after prolonged subculture (41). Interestingly, propagation of CAV21 in ICAM-La-4 cells, in contrast to ICAM-L5 cells, was severely depressed (Fig. 2D). This suggested that CAV21 shares the known host restrictions of HRVs in murine cells, at least in representative targets derived of RT epithelium.

We performed serial passages of CAV21 in ICAM-La-4 cells to investigate whether *in vitro* adaptation might yield mouse RT-competent virus. After 10 alternate passages in ICAM-La-4 and HeLa H1 cells, followed by five passages in ICAM-La-4 cells, infection produced prominent cytopathic effects in the latter. Whole-genome sequencing of serially passaged virus after plaque purification revealed three amino acid exchanges mapping to the capsid proteins VP2 (Ser207→Asn) and VP3 (Ala520→Val) and the nonstructural protein 2C (Val1371→Met) (amino acid numbering refers to the CAV21 polyprotein) (Fig. 3A). CAV21 adapted in an RT tissue culture model (CAV-TCA [tissue culture adapted]) containing the three amino acid exchanges was cloned, rederived, and tested

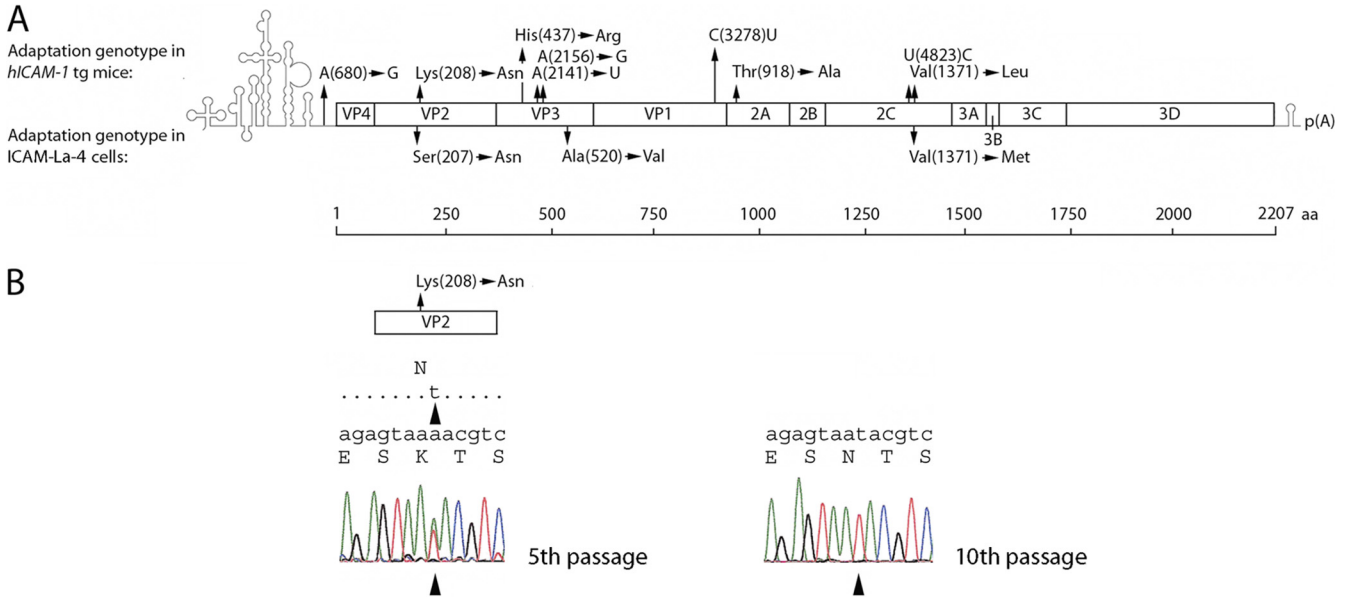

FIG. 3. CAV21 adaptation sequences. (A) (Top) Adaptation genotype determined by population sequencing of virus recovered from the lungs of *hICAM-1* tg mice after 10 *in vivo* passages and amplification in HeLa H1 cells. Nucleotide exchanges in the 5′ UTR and silent mutations in the ORF are indicated by the single-letter abbreviation. Their numbering refers to the nucleotide sequence of the CAV21(Kuykendall) reference strain (GenBank accession no. AF546702.1). Amino acid exchanges are indicated by the three-letter abbreviation, and numbering refers to the CAV21(Kuykendall) polyprotein (bottom). (Middle) Adaptation genotype determined by population sequencing after 10 *in vitro* passages in ICAM-La-4 cells. (B) Evolution of substitution A1337→T resulting in Lys208→Asn in VP2 during serial *in vivo* passage in the lungs of infected *hICAM-1* tg mice. The arrowheads indicate the mutant residue in the chromatogram obtained from population sequencing of virus recovered from the lungs of infected *hICAM-1* tg mice at the indicated passage.

for one-step growth kinetics in ICAM-La-4 cells. The latter revealed similar growth kinetics in ICAM-La-4 and HeLa H1 cells (Fig. 2D). Intratracheal inoculations of recombinant CAV-TCA in groups of *hICAM-1* tg mice conducted as outlined above (Fig. 1B) revealed a pattern of viral clearance by 24 h postinoculation similar to its wt CAV21 parent (data not shown). This suggested that the adaptation of CAV21 *in vitro* is not sufficient to overcome the intracellular block to viral replication in the murine RT epithelium.

***In vivo* adaptation of CAV21 to mouse RT epithelium.** Since neither wt nor ICAM-La-4-adapted CAV21 exhibited efficient replication in the murine RT, we embarked on *in vivo* adaptation of the virus in the lungs of *hICAM-1* tg mice. This strategy was motivated by two observations. First, rapid clearance of the inoculum only in tg animals by 6 h postinoculation and experiments with anti-ICAM-1 antibodies indicated eclipse of virus and, thus, successful entry and uncoating upon binding to hICAM-1 on RT epithelial cells. Second, a delicate but consistent increase in viral titers isolated 10 h versus 6 h postinoculation (Fig. 1D) suggested marginal propagation of the virus. Thus, serial passage of CAV21 in *hICAM-1* tg mouse lungs might select for RT-competent variants.

Two *hICAM-1* tg mice were infected by the i.t. route with 2×10^5 PFU of wt CAV21. Twenty-eight (for passages 1 to 4) or forty-eight (for passages 5 to 10) hours postinoculation, lungs were dissected and homogenized, and titers were quantified by plaque assay. The incubation period was extended due to improved recovery of virus beyond 28 h after infection with passages 5 and higher (Fig. 4B) to encourage genetic adaptation. Lung homogenates from the animal with the highest intrapulmonary titer were used to inoculate HeLa H1 cells. Virus amplified in this manner was quantified by plaque assay and used to inoculate a subsequent pair of *hICAM-1* tg mice in an identical fashion. This procedure was repeated 10 times. Plaque assays of lung homogenates from the first 5 passages revealed emergence of a large-plaque variant by the 2nd passage (Fig. 4A). The proportion of large-plaque variants steadily increased, and they dominated the sample by the 5th passage (Fig. 4A). The amounts of virus recovered 48 h postinoculation increased significantly with serial passages 6 to 10 (Fig. 4B). Since the evolution of an altered plaque phenotype was complete by passage 5 and virus yields did not increase beyond passage 8 (Fig. 4B), the *in vivo* adaptation procedure was halted at passage 10.

A mouse-adapted strain of CAV21. Serial-passaged CAV21 recovered from infected mouse lungs was propagated in HeLa H1 cells after the 5th and 10th passages, and the entire genome was sequenced using viral RNA isolated from bulk virus (population sequencing) as described in Material and Methods. At 5 passages, population sequencing revealed a number of single nucleotide polymorphisms. There was considerable heterogeneity at mutated nucleotides, judging by the appearance of multiple overlapping peaks of similar magnitude in the chromatogram (Fig. 3B). Due to obvious genetic heterogeneity of *hICAM-1* tg mouse lung-derived virus populations and because maximum virus recovery had not been reached after 5 passages, no attempts were made to isolate or clone large-plaque virus variants.

At passage 10, population sequencing revealed that all mutations identified in Fig. 3A were dominant, with the area

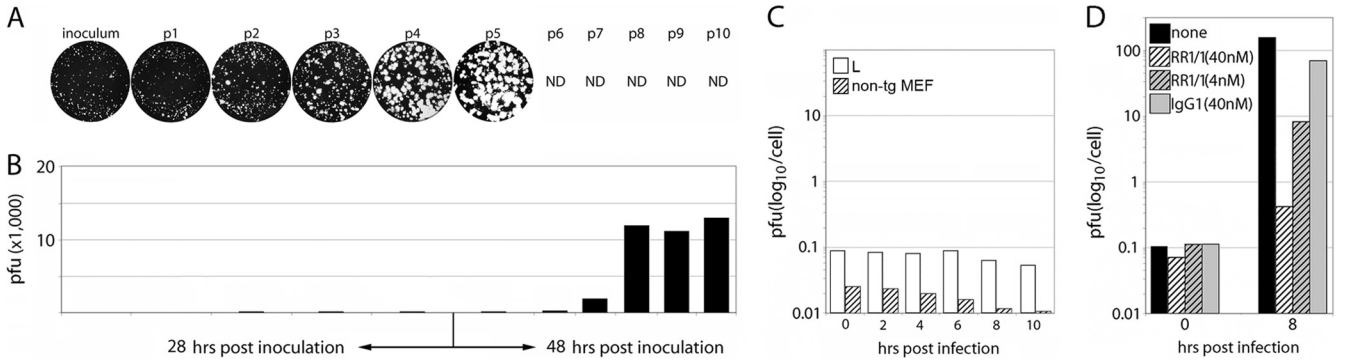

FIG. 4. Evolution of variant plaque phenotype/virus recovery in *hICAM-1* tg mouse lungs. (A) Two male *hICAM-1* tg mice were infected with wt CAV21 (inoculum) or passaged (p1 to p10) virus by the i.t. route. Virus recovered 28 h (for passages 1 to 4) or 48 h (for passages 5 to 10) after inoculation was amplified in HeLa H1 cells. Plaque assays show virus analyzed after amplification of each passage in HeLa H1 cells. The plaque phenotype did not change after passage 5. (B) Total CAV21 titers recovered 28 h (passages 1 to 4) or 48 h (passages 5 to 10) after i.t. injection from *hICAM-1* tg mouse lung homogenates at individual passages. The values shown represent averages from both infected animals per passage. (C) One-step growth kinetics of CAV-RTA in mouse L fibroblasts (L) and in *hICAM-1* tg-negative mouse embryonic fibroblasts (non-tg MEF). (D) CAV-RTA propagation in HeLa H1 cells pretreated with medium alone (none) or medium containing the indicated antibodies at the concentrations given.

under the "mutant peak" >90% of the total at the position in the chromatogram. This phenomenon is shown for the evolution of the exemplary Lys208→Asn mutation in VP2 from passage 5 to passage 10 (Fig. 3B). Plaque-purified virus from passage 10 was sequenced, and the genomic sequence contained all dominant mutations that were previously identified by population sequencing of virus at passage 10 (Fig. 3A). This finding and the absence of obvious single nucleotide polymorphisms in the population sequence at passage 10 suggest that after 10 passages in the lungs of *hICAM-1* tg mice, a predominant CAV21 genotype had emerged. However, we cannot exclude minor genetic heterogeneity in the pool of viruses obtained from *hICAM-1* tg mouse lungs, and no attempts were made to systematically evaluate the precise composition of the virus population. The dominant mutant virus with the genotype shown (CAV-RTA [respiratory tract adapted]) (Fig. 3A) was cloned and rederived for further tests.

Several observations from genetic analyses of CAV-RTA stand out. There were clear similarities with CAV-TCA obtained after serial passage in ICAM-La-4 cells (Fig. 3A). All viral proteins that acquired adaptation mutations for growth in ICAM-La-4 cells (VP2, VP3, 2C) also were altered in CAV-RTA. A mutation in the capsid protein VP2, Lys208→Asn in CAV-RTA, was directly adjacent to Ser207→Asn in CAV-TCA (Fig. 3A). Also, a mutation in the nonstructural protein 2C, Val1371→Leu in CAV-RTA, was Val1371→Met in CAV-TCA (Fig. 3A). We identified four nucleotide exchanges in CAV-RTA that, in addition to one mutation in the 5′ UTR, did not result in amino acid substitutions (Fig. 3A). As with nucleotide exchanges resulting in coding alterations, there was genetic heterogeneity at these positions at passage 5, which evolved into the dominant, seemingly homogeneous genotype at passage 10. It is therefore plausible that silent nucleotide substitutions may contribute to mouse RT adaptation of CAV-RTA. None of the mutations, silent or coding, mapped to known *cis*-acting genetic elements involved in genome replication, e.g., the *cis*-acting replication element (*cre*), which (in CAV21) resides in the 2C ORF (36).

Since CAV-RTA acquired mutations in VP2 and VP3, capsid proteins that participate in interactions with hICAM-1, we evaluated the possibility of adaptation to an alternative murine receptor. As with wt CAV21 (14) (Fig. 2B), there was no propagation of CAV-RTA in mouse L fibroblasts or mixed fibroblast cultures prepared from *hICAM-1* tg-negative mouse embryos (14) (Fig. 4C). Furthermore, CAV-RTA responded to receptor blockage with RR1/1 antibody pretreatment of HeLa H1 cells (Fig. 4D) in a manner similar to that of wt CAV21 (Fig. 1D). This suggested that CAV-RTA cell attachment and entry did not occur in mouse cells in the absence of hICAM-1 and required hICAM-1 in human cells.

In principle, the selection of CAV-RTA through serial passage in the lungs of *hICAM-1* tg mice could have been influenced by intermittent passage in HeLa H1 cells (used to amplify virus obtained from lung lysates). However, CAV-RTA exhibited diminished propagation potential in HeLa H1 cells (Fig. 5). Cloned CAV-RTA produced substantially enlarged plaques (data not shown), recapitulating the plaque phenotype observed with virus recovered from the lungs of infected *hICAM-1* tg mice at passage 5 and beyond (Fig. 4A). Both wt CAV21 and CAV-RTA reached maximum progeny yields by 5 to 6 h after infection of HeLa H1 cells (Fig. 5A). However, CAV-RTA achieved only ~20% of the wt yield (Fig. 5A). EV proteases 2A and 3C target eukaryotic initiation factor (eIF) 4G (15) and poly(A)-binding protein (PABP) (26) in infected host cells. The degradation of target host translation factors in HeLa H1 cells (Fig. 5B) was slowed by ~2 h with CAV-RTA compared to that of the wt CAV21. Accordingly, translation of CAV-RTA proteins, such as the nonstructural viral protein 2C, was similarly delayed (Fig. 5B). This suggests that CAV-RTA has inherently lower propagation potential in HeLa H1 cells than wt CAV21, thus excluding intermittent HeLa H1 passage as a factor in the selection for the CAV-RTA genotype.

Propagation of CAV-RTA in the lungs of *hICAM-1* tg mice. We consistently observed slightly elevated (~2-fold) average recovery of wt CAV21 at 10 h after i.t. inoculation compared to that at the 8-h interval (Fig. 1C). Also, virus recovery from the

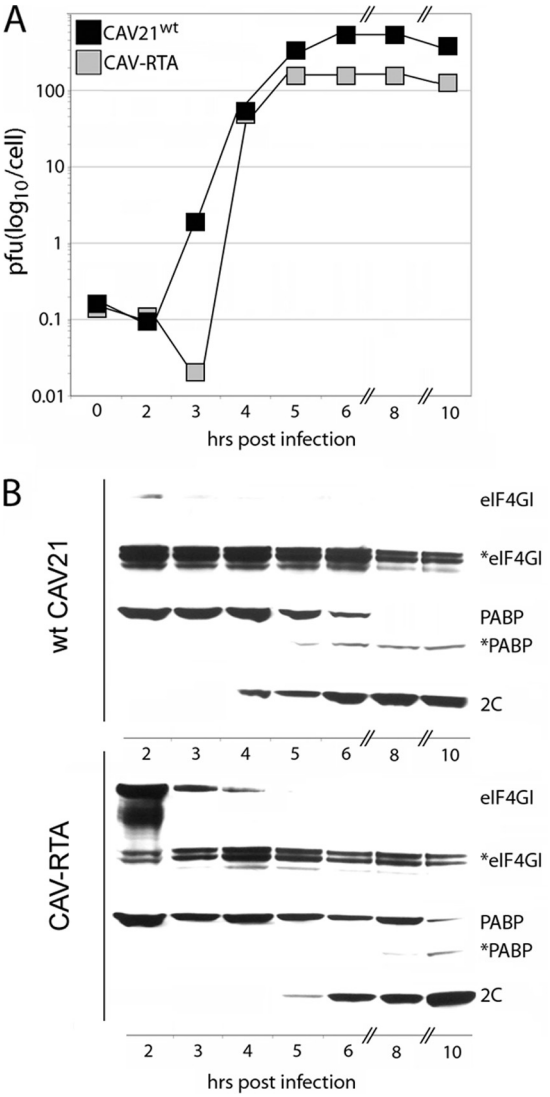

FIG. 5. Growth properties of CAV-RTA in HeLa H1 cells. (A) One-step growth kinetics of wt CAV21 and cloned, recombinant CAV-RTA in HeLa H1 cells. (B) Cleavage of eIF4G1 and PABPC1 in CAV21/CAV-RTA-infected HeLa H1 cells (asterisks indicate cleavage products recognized by antibodies detecting the intact proteins) and expression of the viral 2C protein.

lungs of all four mice in the 10-h experimental groups was higher than any of the mice in the 8-h groups. This suggests that marginal viral replication may take place after internalization of wt CAV21 into RT epithelial cells. We tested whether *in vivo* adaptation resulted in enhanced CAV-RTA recovery of virus after i.t. inoculation. To this end, we conducted experiments similar to those shown in Fig. 1D, where virus was coinoculated by the i.t. route with antibodies. We carried out i.t. inoculations of CAV-RTA in four male *hICAM-1* tg mice or non-tg littermates per group with 2×10^5 PFU of virus in the presence of RR1/1 antibody or control, isotype-matched nonspecific mouse IgG. The animals were euthanized at the intervals shown, and viral titers from lung homogenates were determined (Fig. 6A).

Recovery of CAV-RTA in the control *hICAM-1* tg group at 10 h after i.t. inoculation slightly exceeded the inoculum and was higher than that in non-tg mice, suggesting that virus propagation had occurred (Fig. 6A). The presence of RR1/1 antibody reduced virus recovery at all intervals up to 48 h postinoculation (Fig. 6A). This is in contrast to wt CAV21, where the addition of RR1/1 enhanced virus recovery, presumably by preventing virus eclipse and, thus, increasing the isolation of input virus from infected lungs (Fig. 1B). Anti-hICAM-1 antibody had the opposite effect on CAV-RTA, indicating that blocked entry may result in diminished virus recovery 10 to 48 h after i.t. inoculation due to prevention of viral entry and subsequent replication in RT epithelium. Recovery of CAV-RTA was possible up to 96 h postinoculation (Fig. 6A), while we were unable to isolate wt CAV21 from infected lungs of *hICAM-1* tg mice as early as 48 h postinfection (Fig. 1B). Also, recovery of CAV-RTA 48 h after infection and beyond slightly exceeded the levels observed with non-tg mice. CAV-RTA recovery from non-tg mice paralleled the results with wt CAV21 at all intervals tested, confirming that CAV-RTA did not acquire specificity for an endogenous murine receptor (Fig. 6A). Our experiments suggest that serial *in vivo* passage of CAV21 after i.t. injection in *hICAM-1* tg mice produced an altered genotype which exhibits replication capacity in RT epithelium of *hICAM-1* tg mice.

Virus recovery of CAV-RTA from the lungs of infected *hICAM-1* tg mice suggested hICAM-1-dependent, active viral replication in the respiratory tract. However, these findings provide only indirect evidence for viral propagation. To directly demonstrate viral replication in the murine RT, we probed infected lung lysates for immunoblotting of viral nonstructural proteins. Male *hICAM-1* tg mice or their non-tg littermates were infected with wt CAV21 or CAV-RTA by the i.t. route. Since this assay did not involve virus recovery from lungs and to maximize production of viral nonstructural proteins, we increased the inoculum to 2×10^7 PFU. One mouse each was euthanized at defined intervals, and the dissected lungs were processed and fractionated for immunoblotting (see Materials and Methods). In *hICAM-1* tg mice, i.t. inoculation of CAV-RTA revealed the presence of ~130-kDa and ~82-kDa products reactive with a polyclonal antibody raised against the 3D RNA-dependent RNA polymerase of poliovirus (cross-reactivity of the antibodies was confirmed with immunoblot of CAV21-infected HeLa H1 cell lysates [data not shown]). The protein bands were detected at 8 h postinfection and increased in intensity toward 24 h (Fig. 6B, lanes 8 to 11), in accordance with the kinetics of CAV-RTA recovery from the lungs of infected tg mice (Fig. 6A). Analyses of lung lysates from CAV-RTA-infected non-tg littermates did not reveal signal beyond the background stain observed in lung lysates from all animals (Fig. 6B, lanes 12 to 15), including noninfected *hICAM-1* tg mice (Fig. 6B, lanes 1 to 3). We also failed to detect a corresponding signal in *hICAM-1* tg mice infected with wt CAV21 (Fig. 6B, lanes 4 to 7).

We used a stepwise fractionation procedure to process lung lysates (see Materials and Methods). The CAV-RTA-associated signal in lung lysates from *hICAM-1* tg mice was detected when using material from pellets obtained after centrifugation of cytoplasmic extracts (Fig. 6B) but not in supernatants representing cytoplasmic fractions (data not shown). This suggests that the detected proteins remain associated with membranous

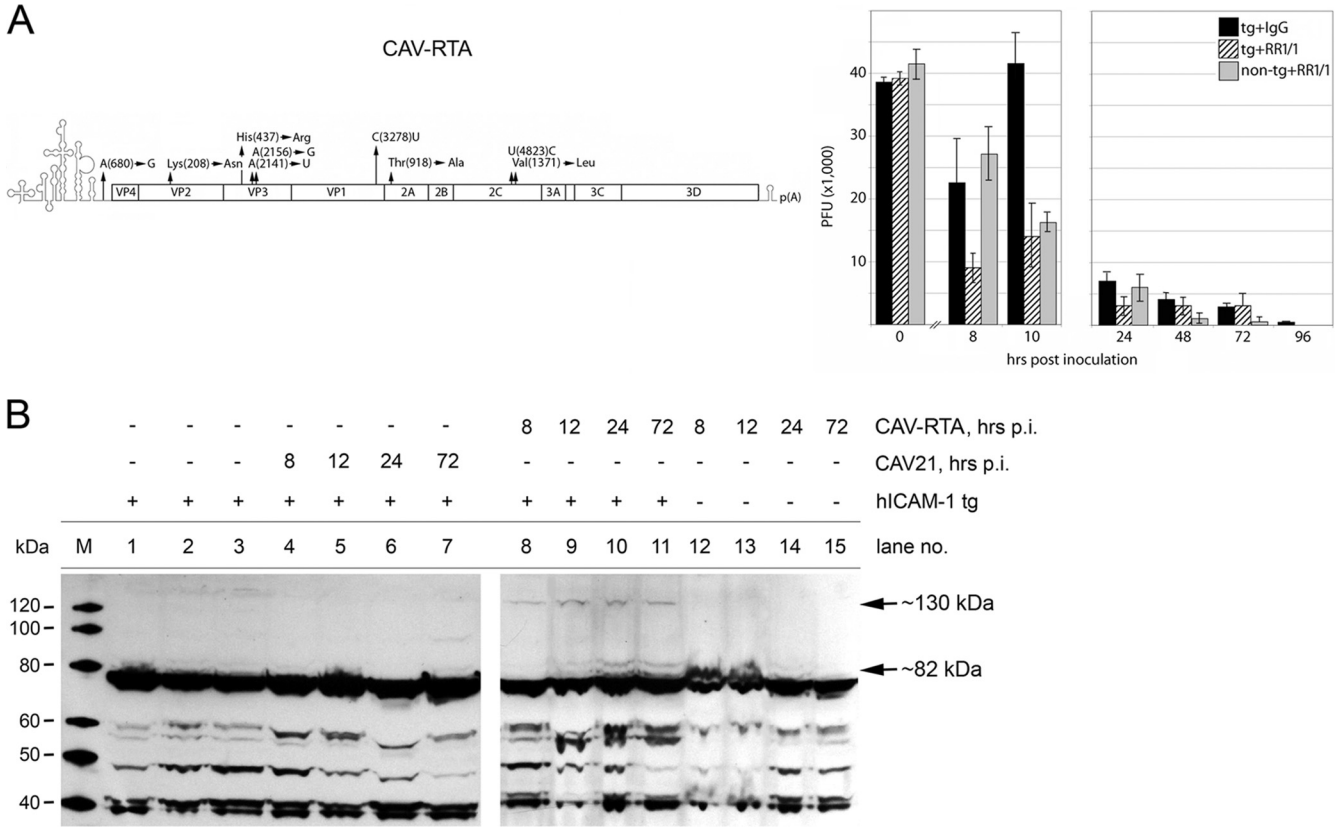

FIG. 6. Propagation of CAV-RTA in the RT of *hICAM-1* tg mice. (A) Virus recovered from lungs of mice inoculated with 2×10^5 PFU of CAV-RTA up to 10 h (left) and 96 h (right) after i.t. infection. Groups of male *hICAM-1* tg mice or non-tg littermates ($n = 4$) were inoculated i.t. with virus in the presence of antibodies (40 nM) as indicated and tested for virus recovery from lungs at the intervals shown. The values represent the average recovered amounts of virus from the animals in each group. The bars indicate the standard deviations. (B) Immunoblot of mouse lung lysates with rabbit polyclonal antibodies recognizing CAV21 3D. Lysates were obtained from mock-infected *hICAM-1* tg mice (lanes 1 to 3), wt CAV21-infected *hICAM-1* tg mice (lanes 4 to 7), CAV-RTA-infected *hICAM-1* tg mice (lanes 8 to 11), or CAV-RTA-infected non-tg mice (lanes 12 to 15). All mice were infected by the i.t. route. Two immunoreactive bands at ~130 and ~82 kDa are indicated. The experiment was repeated three times; a representative assay is shown.

fractions resistant to mild detergent treatment in the lysis buffer used (see Materials and Methods). These findings are consistent with detection of CAV21 precursor polypeptides, including the 3D polymerase. Since it comigrates with strong background bands at ~50 kDa, we were unable to determine whether mature, processed 3D is present in infected lung lysates. We attempted to verify the identity of the precursor polypeptides via incubation of lung lysates with recombinant poliovirus 3CD protease. To this end, we homogenized lung tissues and processed lysates in buffer lacking protease inhibitors. This assay failed, because no 3D antibody-reactive bands were recovered in any samples, suggesting spontaneous degradation of the material.

To determine if CAV-RTA infection produces RT histopathology in *hICAM-1* tg mice, we carefully examined lungs from i.t. inoculated animals. Four male *hICAM-1* tg mice each were infected with 2×10^7 PFU CAV-RTA or wt CAV21 by the i.t. route. For controls, four non-tg peers were inoculated with CAV-RTA in the same manner. The lungs of inoculated mice were excised 96 h after i.t. infection and processed for histopathological analysis. The lungs were sectioned *in toto*, and hematoxylin and eosin (H&E)-stained sections were carefully examined for histopathological lesions. CAV-RTA failed to produce overt histopathological lesions in the lungs of i.t. infected *hICAM-1* tg mice. This is in accordance with similar findings for the upper RT with analogous experimental EV infections of human volunteers (43, 44).

Previous mouse adaptation strategies with HRVs *in vitro* revealed adaptation mutations mapping to the coding region for the viral P2 proteins, 2B and 2BC (24, 47), or the P3 protein, 3A (23). However, in our *in vitro* approach in ICAM-La-4 cells or in *hICAM-1* tg mice *in vivo*, adaptation mutations occurred in the coding region for the VP2 and VP3 capsid proteins (Fig. 3). To test the functional significance of these in mouse RT competence, a variant of CAV-RTA containing the wt CAV21 capsid (termed CAV-RTB) was tested in *hICAM-1* tg mice (Fig. 7A). We tested i.t. inoculation of CAV-RTB in *hICAM-1* tg mice by using the template described in Fig. 1B. Virus recovery from *hICAM-1* tg mouse lungs followed the trajectory observed with wt CAV21 (Fig. 7A; also compare Fig. 1B and D). This indicates that adaptation mutations in nonstructural proteins alone are insufficient to mediate CAV21 replication in the mouse RT.

Adaptation mutations mapping to the viral capsid proteins

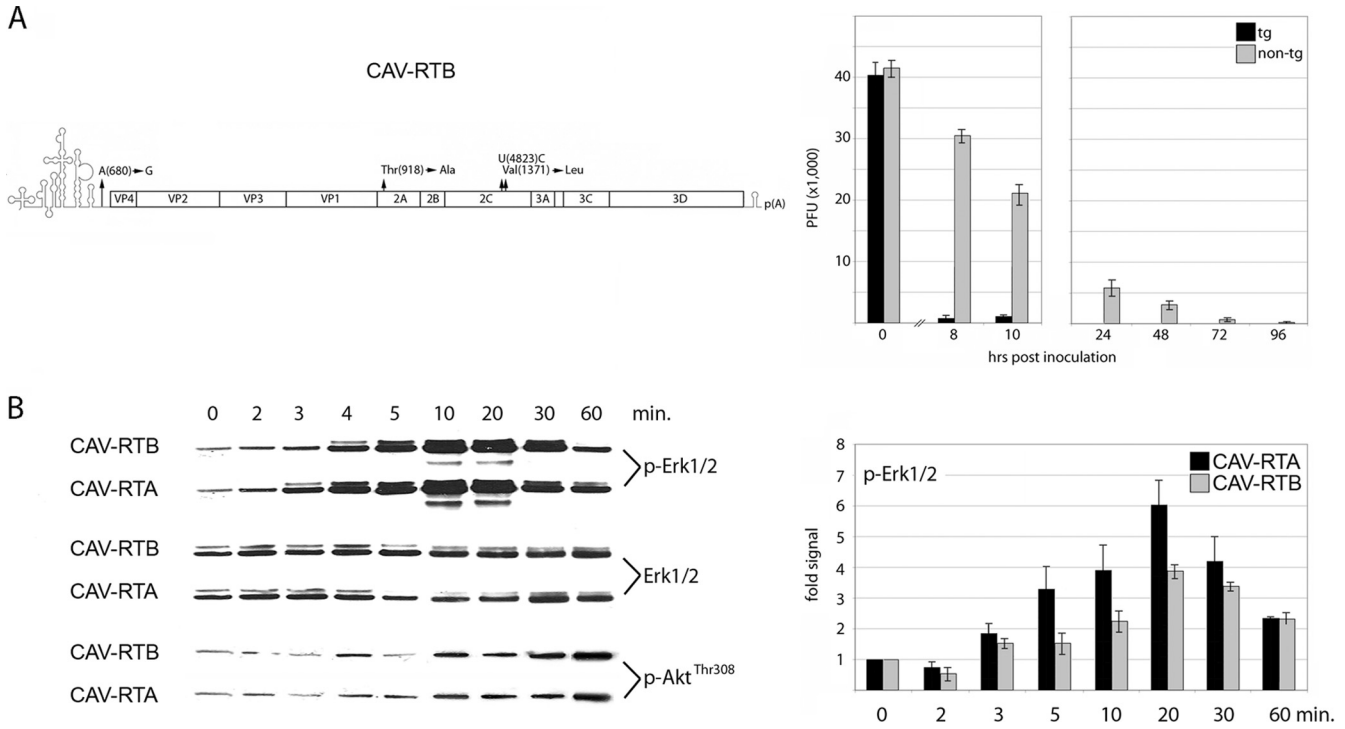

FIG. 7. The effect of CAV-RTA capsid mutations on viral RT competence. (A) Virus recovered from lungs of mice inoculated with 2×10^5 PFU of CAV-RTB up to 10 h (middle) and 96 h (right) after i.t. infection. Groups of male *hICAM-1* tg mice or non-tg littermates ($n = 4$) were inoculated i.t. with CAV-RTB as indicated and tested for virus recovery from lungs at the intervals shown. The values represent the average recovered amounts of virus from the animals in each group. The bars indicate the standard deviations. (B) (Left) Erk1/2 and Akt(Thr308) phosphorylation after binding of CAV-RTA or -RTB to serum-starved HeLa H1 cells (the data are a representative series of results from three independent assays). (Right) Densitometry of p-Erk1/2 immunoblots. The mean values from results of two independent assays are shown; bars indicate standard deviations.

may contribute to mouse RT competence by facilitating intracellular events, such as particle morphogenesis (31). However, since adaptation mutations identified in our screen map to regions of VP2 and VP3 involved in interactions with the ICAM-1 receptor (45), it was plausible that adaptation mutations may alter virus-receptor contacts. Binding of ligands, including HRVs, to the ICAM-1 receptor elicits signal transduction events (reviewed in reference 30). Thus, altered CAV21–ICAM-1 interactions upon adaptation to the mouse RT may facilitate virus propagation via changes in downstream signal transduction. Our focus was on Erk1/2 mitogen-activated protein kinases (MAPK), which are prominent downstream targets of hICAM-1 signaling (18). We recently reported that Erk1/2 signaling to a downstream substrate, the MAPK signal-integrating kinase 1 (Mnk1), stimulates viral, cap-independent translation at the internal ribosomal entry site (IRES) of HRV2 (19). It is therefore possible that CAV21–ICAM-1 interactions and the resulting downstream signal may influence early events in the viral life cycle, e.g., translation of the viral polyprotein.

Erk1/2 phosphorylation kinetics upon CAV21 binding to serum-starved HeLa H1 cells were commensurate with an hICAM-1-mediated event. Phosphorylation was first noted after ~3 to 4 min, peaked at ~10 to 20 min, and waned by ~60 min after virus addition to cell media. There were moderate but reproducible differences attributable to the CAV-RTA capsid (Fig. 7B). Activation of Erk1/2 occurred earlier, produced higher phospho-Erk1/2 levels, and persisted longer with CAV-RTA (Fig. 7B, right). This was not due to changes in overall Erk1/2 protein levels (Fig. 7B, left). Also, non-ICAM-1-related signaling events induced by virus infection, e.g., phosphorylation of Thr308 in Akt, occurred much later and were unchanged in CAV-RTA compared to CAV-RTB (Fig. 7B). Our observations suggest that the CAV-RTA capsid may alter virus–ICAM-1 interactions, resulting in changed hICAM-1 signaling kinetics upon virus binding.

DISCUSSION

The principal impediments to a mouse model for EV RT infection are intracellular host restrictions to virus replication (23, 24, 47). Therefore, our empirical strategy was strictly centered on investigating EV propagation in the RT of *hICAM-1* tg mice and not the nature or extent of the host response to infection (1). Wt CAV21, while readily capable to propagate in mouse L fibroblasts expressing hICAM-1, is severely growth deficient in hICAM-1-expressing murine cells of RT origin (La-4). Thus, host range restrictions to EV RT replication may be poorly retained in dedifferentiated, high-passage tissue culture systems, such as L cells. Failure of La-4-adapted CAV21 to propagate in the RT of *hICAM-1* tg mice suggests that even authentic, mouse RT-derived cell culture systems may not properly represent the target in the live organism. Therefore, to obtain mouse RT-competent EVs, there may be few alter-

natives to the *in vivo* adaptation procedure through serial passage in the lungs of *hICAM-1* tg mice adopted here.

Our experiments with wt CAV21 inoculated in *hICAM-1* tg mice by the i.t. route suggest that efficient, hICAM-1-dependent virus uptake and eclipse occur in mouse RT epithelial cells. The failure to recover significant amounts of virus from lungs later than 24 h postinfection implies an intracellular replication block at a postuncoating step in mouse RT epithelium. Since uncoating of the wt CAV21 genome presumably occurs in mouse RT epithelium, the viral genome represents a quasi-infectious RNA that might acquire adaptation mutations through our serial *in vivo* adaptation strategy. Indeed, serial passage of wt CAV21 in the RT of *hICAM-1* tg mice produced large-plaque variants that continuously evolved in subsequent passages into a dominant adaptation genotype, CAV-RTA.

Since our main empirical tool to detect RT propagation is virus recovery from infected lungs, enhanced CAV-RTA isolation may reflect passive selection of a genotype able to persist in the RT rather than genetic adaptation through active replication. However, a number of observations argue in favor of the latter. CAV-RTA forms plaques that are significantly larger than the range of plaque sizes observed with wt virus. This suggests that CAV-RTA must have newly emerged in *hICAM-1* tg mice through genetic variation, implying active replication. CAV-RTA's slight but distinct growth disadvantage in HeLa H1 cells excludes positive selection during intermittent amplification in HeLa H1 cells as a factor in adaptation. CAV-RTA exhibited genetic variation affecting the same viral polypeptides (VP2, VP3, 2C) and, in some instances, the same or adjacent amino acids as ICAM-La-4-adapted virus. Intriguingly, mutation of Val1371 was unanimous in ICAM-La-4 and CAV-RTA, but it was changed to Met in the former and Leu in the latter. The fact that genetic adaptations in ICAM-La-4 cells, undoubtedly a result of active viral RNA replication, and in the RT of *hICAM-1* tg mice produced similar polymorphisms strongly suggests a common mechanism giving rise to these variants. In other words, if Val1371→Met enables CAV21 replication in ICAM-La-4 cells *in vitro*, it is likely that Val1371→Leu serves a similar purpose in the mouse RT *in vivo*. Similar but clearly distinct genotypes of La-4-adapted virus and CAV-RTA exclude the possibility of laboratory contamination. Added genetic variation in CAV-RTA compared to that of La-4-adapted virus may explain the failure of the latter to replicate in the RT of *hICAM-1* tg mice. CAV-RTA failed to replicate in wt mouse L fibroblasts or in embryonic fibroblasts from non-tg mice, and CAV-RTA replication was effectively blocked by RR1/1 anti-ICAM-1 antibody pretreatment of HeLa H1 cells. This indicates that *in vivo* adaptation to an alternative, murine cell receptor was unlikely. Furthermore, the recovery of CAV-RTA from the lungs of infected non-tg animals followed the same trajectory as that of wt CAV21, indicating that adaptation did not alter virus-host interactions in the absence of hICAM-1.

CAV-RTA infection of *hICAM-1* tg mice by the i.t. route led to the expression of viral nonstructural polypeptides in lungs. We deliberately avoided immunohistochemistry, because generally low viral propagation levels possibly diffuse distribution of infected cells, and notorious problems with false-positive signal limit this approach. Immunoblot analyses of lung lysates from *hICAM-1* tg mice infected with CAV-RTA revealed the presence of distinctive bands immunoreactive with antibodies recognizing the 3D polymerase of CAV21. Importantly, this signal was not obtained in similar assays of the lungs of CAV-RTA-infected non-tg littermates. We hypothesize that the detected proteins represent unprocessed precursor polypeptides containing the 3D polymerase. This may indicate delayed CAV21 polyprotein processing in the RT of *hICAM-1* tg mice (compared to HeLa H1 cells), specifically by the viral 3CD protease. Indeed, inhibition of *in vitro* polyprotein processing of poliovirus with anti-3CD antibodies yielded precursor proteins, including P3 and slower-migrating varieties in a pattern reminiscent of our results (22, 42).

Wt CAV21 rapidly and avidly acquired adaptation mutations upon serial passage in the RT of *hICAM-1* tg mice. Our procedure yielded a dominant adaptation genotype with surprisingly little heterogeneity among the virus population isolated from infected mouse lungs. CAV-RTA contained adaptation mutations in the IRES, the coding region for the capsid proteins VP2 and VP3 and the nonstructural proteins 2A and 2C in a single viral genome. This suggests that to overcome the intracellular block to wt CAV21 replication in the murine RT, complex readjustments of virus-host interactions and/or viral functions are required. It is unlikely that any of the mutations identified or the viral functions affected act alone in mediating mouse RT competence. Rather, adaptation mutations in disparate parts of the viral genome affecting distinct viral functions may cooperate in mediating RT competence. One intriguing possibility recently suggested is that CAV21 VP3 and 2C cooperate in particle assembly (31). Since both viral polypeptides are mutated in CAV-RTA, genetic adaptation may benefit particle assembly in a new host species.

The adaptation mutations in the capsid of CAV-RTA are of particular interest. EV receptors are not mere docking sites but provide crucial signals in infected cells that are usurped by invading viruses (11). The pathogenic profile of ICAM-1-tropic EVs and their role in exacerbation of underlying chronic pulmonary disease is defined by their receptor specificity. The fact that *in vitro* and *in vivo* adaptation of CAV21 yielded (similar) capsid protein mutations suggested that mouse adaptation may require altered virus-receptor interactions, possibly resulting in enhanced ICAM-1 signaling upon virus binding. Indeed, CAV-RTA produced moderate but consistently enhanced Erk1/2 activation in serum-starved HeLa H1 cells compared to that of its wt capsid variant CAV-RTB. Such events, possibly of minor functional consequence in transformed laboratory cell lines with constitutively active signal transduction pathways, may be critical in normal RT epithelium. For example, it has been proposed that stimulation of viral, cap-independent translation initiation occurs via activation of Mnk1 (a shared Erk1/2 and p38 MAPK substrate and, hence, ICAM-1 downstream signaling target) (19, 29). Translation of the incoming viral RNA genome is key for timely synthesis of viral proteins that thwart host responses to infection and, thus, may constitute an early, rate-limiting step of the infectious cycle.

Our investigations of CAV21 mouse RT competence have revealed surprisingly complex virus-host relationships that determine viral replication. Our studies provide a first logical step toward unraveling these relationships by generating hICAM-1-tropic EVs capable of replicating in the RT of *hICAM-1* tg mice.

ACKNOWLEDGMENTS

We thank E. Wimmer for providing infectious cDNA for CAV21(Kuykendall) and antibodies against EV nonstructural proteins. We thank C.-W. Chow (University of Toronto, Canada) for critically reading the manuscript.

This work was supported by PHS grant HL 091227 (M.G.).

REFERENCES

1. **Bartlett, N. W., et al.** 2008. Mouse models of rhinovirus-induced disease and exacerbation of allergic airway inflammation. Nat. Med. **14:**199–204.
2. **Berendt, A. R., et al.** 1992. The binding site on ICAM-1 for Plasmodium falciparum-infected erythrocytes overlaps, but is distinct from, the LFA-1-binding site. Cell **68:**71–81.
3. **Bloom, H. H., K. M. Johnson, M. A. Mufson, and R. M. Chanock.** 1962. Acute respiratory disease associated with coxsackie A-21 virus infection. II.Incidence in military personnel: observations in a nonrecruit population. JAMA **179:**120–125.
4. **Cate, T. R., et al.** 1965. Production of tracheobronchitis in volunteers with rhinovirus in a small-particle aerosol. Am. J. Epidemiol. **81:**95–105.
5. **Charles, C. H., et al.** 2003. Prevention of human rhinovirus infection by multivalent *fab* molecules directed against ICAM-1. Antimicrob. Agents Chemother. **47:**1503–1508.
6. **Colonno, R. J., P. L. Callahan, and W. J. Long.** 1986. Isolation of a monoclonal antibody that blocks attachment of the major group of human rhinoviruses. J. Virol. **57:**7–12.
7. **Colonno, R. J., J. E. Tomassini, and P. L. Callahan.** 1987. Isolation and characterization of a monoclonal antibody which blocks attachment of human rhinoviruses, p. 93–102. *In* M. A. Brinton and R. R. Rueckert (ed.), Positive strand RNA viruses. Alan R. Liss, Inc., New York, NY.
8. **Couch, R. B.** 2001. Rhinoviruses, p. 777–797. *In* D. M. Knipe and P. M. Howley (ed.), Fields virology, vol. 1. Lippincott Williams & Wilkins, Philadelphia, PA.
9. **Couch, R. B., T. R. Cate, R. G. Douglas, Jr., P. J. Gerone, and V. Knight.** 1966. Effect of route of inoculation on experimental respiratory viral disease in volunteers and evidence for airborne transmission. Bacteriol. Rev. **30:**517–529.
10. **Couch, R. B., et al.** 1965. Production of illness with a small-particle aerosol of coxsackie A21. J. Clin. Invest. **44:**535–542.
11. **Coyne, C. B., K. S. Kim, and J. M. Bergelson.** 2007. Poliovirus entry into human brain microvascular cells requires receptor-induced activation of SHP-2. EMBO J. **26:**4016–4028.
12. **Dick, E. C.** 1968. Experimental infections of chimpanzees with human rhinovirus types 14 and 43. Proc. Soc Exp. Biol. Med. **127:**1079–1081.
13. **Dobrikova, E. Y., R. N. Grisham, C. Kaiser, J. Lin, and M. Gromeier.** 2006. Competitive translation efficiency at the picornavirus type 1 internal ribosome entry site facilitated by viral *cis* and *trans* factors. J. Virol. **80:**3310–3321.
14. **Dufresne, A. T., and M. Gromeier.** 2004. A nonpolio enterovirus with respiratory tropism causes poliomyelitis in intercellular adhesion molecule 1 transgenic mice. Proc. Natl. Acad. Sci. U. S. A. **101:**13636–13641.
15. **Etchison, D., S. C. Milburn, I. Edery, N. Sonenberg, and J. W. Hershey.** 1982. Inhibition of HeLa cell protein synthesis following poliovirus infection correlates with the proteolysis of a 220,000-dalton polypeptide associated with eucaryotic initiation factor 3 and a cap binding protein complex. J. Biol. Chem. **257:**14806–14810.
16. **Fendrick, A. M., A. S. Monto, B. Nightengale, and M. Sarnes.** 2003. The economic burden of non-influenza-related viral respiratory tract infection in the United States. Arch. Intern. Med. **163:**487–494.
17. **Florez de Sessions, P., E. Dobrikova, and M. Gromeier.** 2007. Genetic adaptation to untranslated region-mediated enterovirus growth deficits by mutations in the nonstructural proteins 3AB and 3CD. J. Virol. **81:**8396–8405.
18. **Gardiner, E. E., and S. E. D'Souza.** 1999. Sequences within fibrinogen and intercellular adhesion molecule-1 (ICAM-1) modulate signals required for mitogenesis. J. Biol. Chem. **274:**11930–11936.
19. **Goetz, C., R. G. Everson, L. C. Zhang, and M. Gromeier.** 2010. MAPK signal-integrating kinase controls cap-independent translation and cell type-specific cytotoxicity of an oncolytic poliovirus. Mol. Ther. **18:**1937–1946.
20. **Greve, J. M., et al.** 1989. The major human rhinovirus receptor is ICAM-1. Cell **56:**839–847.
21. **Hamory, B. H., J. O. Hendley, and J. M. Gwaltney, Jr.** 1977. Rhinovirus growth in nasal polyp organ culture. Proc. Soc. Exp. Biol. Med. **155:**577–582.
22. **Hanecak, R., B. L. Semler, C. W. Anderson, and E. Wimmer.** 1982. Proteolytic processing of poliovirus polypeptides: antibodies to polypeptide P3-7c inhibit cleavage at glutamine-glycine pairs. Proc. Natl. Acad. Sci. U. S. A. **79:**3973–3977.
23. **Harris, J. R., and V. R. Racaniello.** 2005. Amino acid changes in proteins 2B and 3A mediate rhinovirus type 39 growth in mouse cells. J. Virol. **79:**5363–5373.
24. **Harris, J. R., and V. R. Racaniello.** 2003. Changes in rhinovirus protein 2C allow efficient replication in mouse cells. J. Virol. **77:**4773–4780.
25. **Hayden, F. G., J. M. Gwaltney, Jr., and R. J. Colonno.** 1988. Modification of experimental rhinovirus colds by receptor blockade. Antiviral Res. **9:**233–247.
26. **Joachims, M., P. C. Van Breugel, and R. E. Lloyd.** 1999. Cleavage of poly(A)-binding protein by enterovirus proteases concurrent with inhibition of translation in vitro. J. Virol. **73:**718–727.
27. **Johnson, K. M., H. H. Bloom, A. Mufson, and R. M. Chanock.** 1962. Acute respiratory disease associated with coxsackie A-21 virus infection. I. Incidence in military personnel: observations in a recruit population. JAMA **179:**112–119.
28. **Johnston, S. L., et al.** 1995. Community study of role of viral infections in exacerbations of asthma in 9-11 year old children. BMJ **310:**1225–1229.
29. **Knauf, U., C. Tschopp, and H. Gram.** 2001. Negative regulation of protein translation by mitogen-activated protein kinase-interacting kinases 1 and 2. Mol. Cell. Biol. **21:**5500–5511.
30. **Lawson, C., and S. Wolf.** 2009. ICAM-1 signaling in endothelial cells. Pharmacol. Rep. **61:**22–32.
31. **Liu, Y., C. Wang, S. Mueller, A. V. Paul, E. Wimmer, and P. Jiang.** 2010. Direct interaction between two viral proteins, the nonstructural protein 2C and the capsid protein VP3, is required for enterovirus morphogenesis. PLoS Pathog. **6:**e1001066.
32. **Lomax, N. B., and F. H. Yin.** 1989. Evidence for the role of the P2 protein of human rhinovirus in its host range change. J. Virol. **63:**2396–2399.
33. **Naclerio, R. M., et al.** 1988. Is histamine responsible for the symptoms of rhinovirus colds? A look at the inflammatory mediators following infection. Pediatr. Infect. Dis. J. **7:**218–222.
34. **Naclerio, R. M., et al.** 1988. Kinins are generated during experimental rhinovirus colds. J. Infect. Dis. **157:**133–142.
35. **Nicholson, K. G., J. Kent, and D. C. Ireland.** 1993. Respiratory viruses and exacerbations of asthma in adults. BMJ **307:**982–986.
36. **Paul, A. V., E. Rieder, D. W. Kim, J. H. van Boom, and E. Wimmer.** 2000. Identification of an RNA hairpin in poliovirus RNA that serves as the primary template in the in vitro uridylylation of VPg. J. Virol. **74:**10359–10370.
37. **Proud, D., and C. W. Chow.** 2006. Role of viral infections in asthma and chronic obstructive pulmonary disease. Am. J. Respir. Cell Mol. Biol. **35:**513–518.
38. **Seemungal, T. A., R. Harper-Owen, A. Bhowmik, D. J. Jeffries, and J. A. Wedzicha.** 2000. Detection of rhinovirus in induced sputum at exacerbation of chronic obstructive pulmonary disease. Eur. Respir. J. **16:**677–683.
39. **Shafren, D. R., D. J. Dorahy, R. A. Ingham, G. F. Burns, and R. D. Barry.** 1997. Coxsackievirus A21 binds to decay-accelerating factor but requires intercellular adhesion molecule 1 for cell entry. J. Virol. **71:**4736–4743.
40. **Staunton, D. E., et al.** 1989. A cell adhesion molecule, ICAM-1, is the major surface receptor for rhinoviruses. Cell **56:**849–853.
41. **Stoner, G. D., Y. Kikkawa, A. J. Kniazeff, K. Miyai, and R. M. Wagner.** 1975. Clonal isolation of epithelial cells from mouse lung adenoma. Cancer Res. **35:**2177–2185.
42. **Toyoda, H., et al.** 1986. A second virus-encoded proteinase involved in proteolytic processing of poliovirus polyprotein. Cell **45:**761–770.
43. **Winther, B.** 1994. Effects on the nasal mucosa of upper respiratory viruses (common cold). Dan. Med. Bull. **41:**193–204.
44. **Winther, B., et al.** 1984. Histopathologic examination and enumeration of polymorphonuclear leukocytes in the nasal mucosa during experimental rhinovirus colds. Acta Otolaryngol. Suppl. **413:**19–24.
45. **Xiao, C., et al.** 2001. Interaction of coxsackievirus A21 with its cellular receptor, ICAM-1. J. Virol. **75:**2444–2451.
46. **Yin, F. H., and N. B. Lomax.** 1986. Establishment of a mouse model for human rhinovirus infection. J. Gen. Virol. **67:**2335–2340.
47. **Yin, F. H., and N. B. Lomax.** 1983. Host range mutants of human rhinovirus in which nonstructural proteins are altered. J. Virol. **48:**410–418.